



Foam effect on the sea surface emissivity in the 8–14 μm region

Raquel Nicolòs,^{1,2} Vicente Caselles,² Enric Valor,² and César Coll²

Received 24 August 2007; accepted 1 October 2007; published 28 December 2007.

[1] The effect of foam on the sea surface emission has been studied in the microwave region, but its effect on thermal infrared emissivity and temperature has not been sufficiently analyzed in the literature. This paper presents thermal infrared measurements of foam-covered seawaters carried out under controlled conditions using a multichannel radiometer working in the 8–14 μm region. The experimental data show a negligible foam effect at low observation angles but a significant increase of emissivity with foam at angles above 45°. Differences between foam and foam-free emissivities are about +0.04 for observation angles of 65°, depending slightly on the radiometric spectral band. The effect of foam is to reduce the angular variation of seawater emissivity. The foam and foam-free emissivity differences yield to differences up to 2.5 K in terms of sea surface temperature (SST), even larger than 1.2 K when the SST is retrieved from satellite using a split window technique. The correction of the foam effect on emissivity could be performed using an estimate of the fraction of sea covered by foam. This correction could improve the SST retrieval, mainly for measurements at large observation angles.

Citation: Nicolòs, R., V. Caselles, E. Valor, and C. Coll (2007), Foam effect on the sea surface emissivity in the 8–14 μm region, *J. Geophys. Res.*, 112, C12020, doi:10.1029/2007JC004521.

1. Introduction

[2] The effect of foam coverage on water surfaces is still a pending issue in the thermal infrared (TIR) region. Estimating the effect of foam, such as whitecaps from breaking waves and foam streaks, on the seawater TIR emissivity is a difficult task, since studies on the subject seem to be nonexistent and measurements are very sparse. There are several works for the microwave region in the literature [Ulaby *et al.*, 1986; Dombrovskiy and Raizer, 1992; Camps *et al.*, 2005]. Results indicate an increase in emissivity with foam coverage. This conclusion cannot be easily extrapolated to the thermal infrared region [Watts *et al.*, 1996], since wavelength at microwave region is comparable to the foam bubble size and much longer than the water coat thickness, while the infrared wavelength is much shorter than bubble size and similar or greater than the film thickness. Measurements of directional (10° from nadir) hemispherical reflectance of seawater and foam carried out by Salisbury *et al.* [1993] showed that, in the 8–12 μm region at least, the reflectance at nadir is unaffected by the presence of foam (differences between foam and foam-free values lower than ± 0.001 ; see Figure 1). They concluded that a wavelength longer than the water coat thickness and the high absorption in the infrared prevent significant volume scattering, unlike in the visible region, and thus any change in emissivity. Therefore possible effects may be

a consequence of an alteration of the slope distribution, i.e., the sea surface roughness produced by foam [Watts *et al.*, 1996].

[3] In this paper, the foam effect is studied in the 8–14 μm region using measurements carried out during the Foam, Rain, Oil Slicks and GPS Reflectometry (FROG) field experiment [Camps *et al.*, 2005]. Measurements were taken not only at nadir but at several viewing angles ranging from nadir to 65°.

[4] In the next section the experimental setup is explained in detail. Section 3 shows the methodology, and the measurement strategy used to obtain the emissivity of foam and foam-free seawaters is detailed in section 4. Section 5 gives the main results and a discussion about the foam effect on the SST retrieval from satellite, and finally, section 6 summarizes the conclusions.

2. Experimental Setup

[5] The FROG 2003 experiment was performed at the facilities of the Institut de Recerca en Tècniques Agropecuàries (IRTA) using a 3 \times 7 m² pool filled with seawater collected near the coast of Tarragona (Spain). The salinity of the seawater was 34 psu. The pool was nearly totally filled during the measurements, and the effect of the part of the pool walls over the water level was quantified before the campaign. The effect of the walls was negligible since the angle subtended by them was very much lower than the angle subtended by the sky. Additionally, the pool was located in an area of fish farm pools, and thus there were not surrounding objects or buildings that could affect the measurements.

[6] Foam was generated by a network of 104 air diffusers placed at the bottom of the pool, and connected to an air

¹Meteorology Department, Mediterranean Centre for Environmental Studies, Paterna, Spain.

²Department of Earth Physics and Thermodynamics, University of Valencia, Burjassot, Spain.

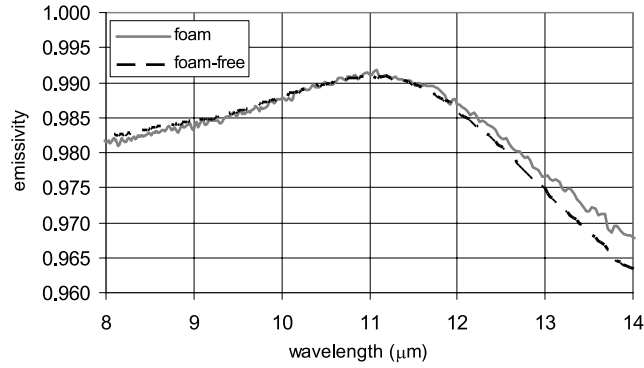


Figure 1. Seawater emissivity calculated from the directional (10°) hemispherical reflectance spectrum measured by *Salisbury et al.* [1993] for the case of a plane surface (solid grey line) and a foam-covered surface (dashed line).

pump with an air flow of $500 \text{ m}^3/\text{h}$ (Figure 2a). Thermal infrared measurements were made with the radiometer CIMEL ELECTRONIQUE model CE 312 [*Legrand et al.*, 2000]. It has four spectral channels: one broadband, $8\text{--}14 \mu\text{m}$ (band 1), and three narrow channels, $8.2\text{--}9.2 \mu\text{m}$, $10.5\text{--}11.5 \mu\text{m}$, and $11.5\text{--}12.5 \mu\text{m}$ (bands 4, 3 and 2, respectively). The radiometer has a field of view of 10° , a response time of 1 s, and accuracies of $\pm 0.10 \text{ K}$, $\pm 0.12 \text{ K}$, $\pm 0.09 \text{ K}$ and $\pm 0.14 \text{ K}$ for channels 1–4, respectively [*Niclòs et al.*, 2004]. The cavity containing the detector is used as a temperature reference. A platinum probe attached to the detector monitors the internal temperature of the head. The radiometer is provided with a concealable, gold coated mirror, which allows comparisons between the radiance coming from an external target and from the optical head cavity in order to check and correct any possible variations in the temperature of the optical head that could affect the measurements. A black body calibration source was used as a reference for the calibration procedure of the radiometer. Extensive calibration measurements were carried out before, during and after the campaign. A calibration function was obtained and applied for each channel.

[7] Six thermistors (see Figure 2b) were located just below the water surface to measure the temperature required to retrieve emissivities using the TIR radiance measurements. They were distributed in the pool so as to show the spatial variability of the temperature, mainly when direct solar radiation over the water surface could affect it. The thermistors were previously calibrated with a thermal bath using a high-accuracy platinum probe. The uncertainty of the six thermistors after the calibration was lower than $\pm 0.1 \text{ K}$ in all cases.

[8] Additionally, a video camera with large angular lens mounted on a periscope was used to acquire foam vertical profiles (see Figure 3b as an example), from which several foam parameters were studied [*Camps et al.*, 2005].

3. Methodology

[9] The radiance measured by the channel i of a TIR radiometer observing the sea surface at ground level in a direction (θ, ϕ) can be expressed as:

$$L_i(\theta, \phi) = \varepsilon_i(\theta, \phi)B_i(T) + L_i^{ref}(\theta, \phi) \quad (1)$$

where $B_i(T)$ is averaged Planck's function for the channel i and a skin temperature T ; $\varepsilon_i(\theta, \phi)$ is the directional sea surface emissivity; and $L_i^{ref}(\theta, \phi)$ is the reflection of the downwelling sky radiance on the sea, which is given by:

$$L_i^{ref}(\theta, \phi) = \int_0^{2\pi} \int_0^{\pi/2} f_{b,i}(\theta', \phi', \theta, \phi) L_{i,atm}^\downarrow(\theta', \phi') \cos \theta' \sin \theta' d\theta' d\phi' \quad (2)$$

where $L_{i,atm}^\downarrow(\theta', \phi')$ is the incident sky radiance in the direction (θ', ϕ') , and $f_{b,i}(\theta', \phi', \theta, \phi)$ is the bidirectional reflectance distribution function (BRDF), which is related with the directional emissivity by:

$$\varepsilon_i(\theta, \phi) = 1 - \int_0^{2\pi} \int_0^{\pi/2} f_{b,i}(\theta', \phi', \theta, \phi) \cos \theta' \sin \theta' d\theta' d\phi' \quad (3)$$

Two approximations are usually used for the surface reflection: Lambertian reflection or specular reflection. If the surface is Lambertian in reflection, $f_{b,i}(\theta', \phi', \theta, \phi) = \rho_{dh,i}/\pi$, $\rho_{dh,i}$ being the directional-hemispherical reflectance, and the reflection term can be rewritten as follows:

$$L_i^{ref}(\theta, \phi) = \frac{1 - \varepsilon_i(\theta, \phi)}{\pi} E_{i,atm}^\downarrow \quad (4)$$

where $E_{i,atm}^\downarrow$ is the sky irradiance, which is defined as:

$$E_{i,atm}^\downarrow = \int_0^{2\pi} \int_0^{\pi/2} L_{i,atm}^\downarrow(\theta', \phi') \cos \theta' \sin \theta' d\theta' d\phi' \quad (5)$$

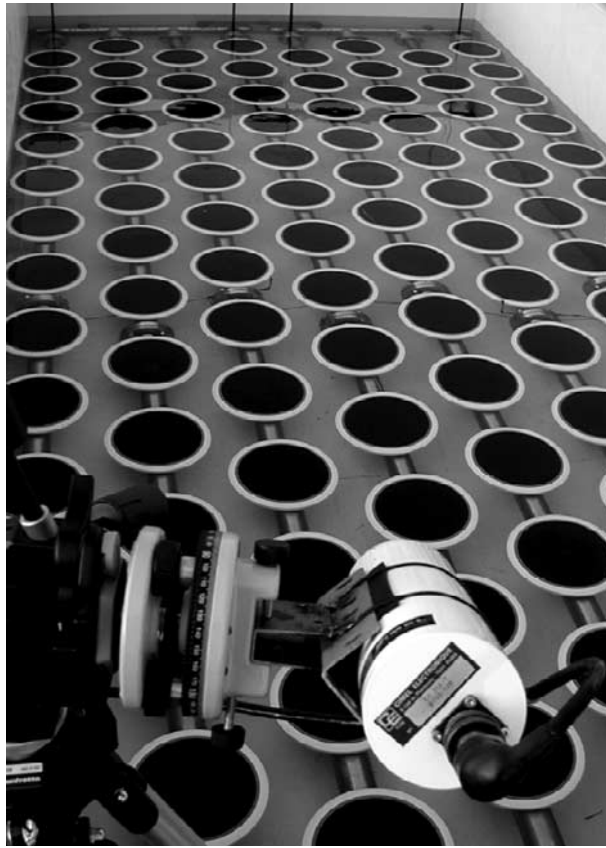
[10] According to equation (5), the measurement of this sky irradiance involves performing a scanning of the atmospheric radiance varying the zenith and azimuth angles of observation in small steps. This process is very lengthy, and the retrieved irradiance could not be ever exactly simultaneous to the water measurements because of the long time required. In order to avoid this lengthy scanning process, there are approximate methods.

[11] The sky radiance $L_{i,atm}^\downarrow(\theta', \phi')$ can be retrieved, in the case of horizontal homogeneity of the atmosphere, i.e., $L_{i,atm}^\downarrow(\theta', \phi') = L_{i,atm}^\downarrow(\theta')$ for totally cloud-free or cloudy skies, as [*Rubio et al.*, 1997]:

$$L_{i,atm}^\downarrow(\theta') \approx L_{i,atm}^\downarrow(0^\circ) \cos^{-x_i}(\theta') \quad (6)$$

where the coefficient x_i varies slightly with the atmospheric conditions and the measurement spectral band. This equation, together with equation (5), gives an approximation for the sky irradiance as:

$$\frac{E_{i,atm}^\downarrow}{\pi} \approx \frac{2}{2 - x_i} L_{i,atm}^\downarrow(0^\circ) \quad (7)$$



(a)



(b)

Figure 2. (a) Air diffusers at the pool bottom and the CE 312 radiometer. (b) Detail of the thermistors located below the water surface.

[12] Additionally, we can use the well-known diffusive approximation [Kondratyev, 1969]:

$$E_{i\ atm}^\perp \approx \pi L_{i\ atm}^\perp(\theta_{ef}) \quad (8)$$

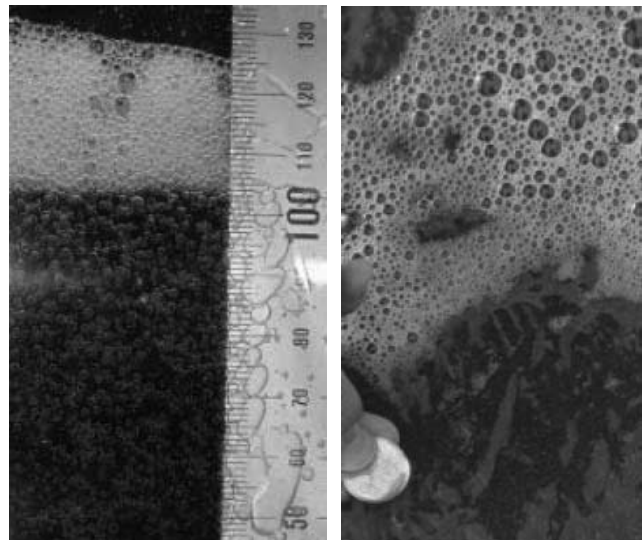
where θ_{ef} is considered as an atmospheric effective angle, which also varies with the atmospheric conditions and the measurement spectral band. Taking into account equations (7) and (8), this effective angle can be retrieved as:

$$\theta_{ef} \approx \arccos \left[\left(\frac{2 - x_i}{2} \right)^{1/x_i} \right] \quad (9)$$

Therefore the $E_{i\ atm}^\perp$ is approximately π times the sky radiance measured at an effective angle θ_{ef} (of about 53° from zenith) for totally cloud-free atmospheres [Kondratyev, 1969]. We carried out some cloud-free sky measurements in order to check the suitability of using these approximations. Simulations of atmospheric magni-



(a)



(b)

(c)

Figure 3. (a) Foam coverage during the FROG experiment. Vertical profiles of the (b) artificially generated foam during the FROG experiment (SSS = 34 psu) and (c) naturally generated foam in the coasts of the Gran Canaria island after wave breaking (scale: 50 euro cent coin, radius = 12 mm) [Camps et al., 2005].

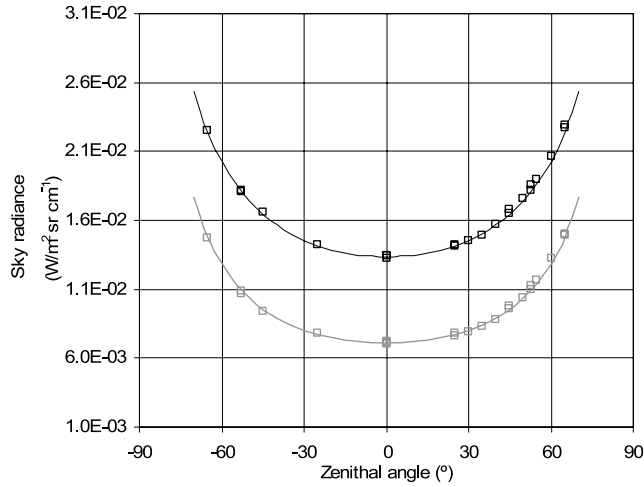


Figure 4. Downwelling sky radiance measured during the experiment (points) and calculated using equation (6) with the x_i values obtained for a midlatitude standard atmosphere (lines). Values for the CE 312 channels 1 and 3 are plotted in black and grey, respectively.

tudes were also computed with the MODTRAN 4 code [Berk *et al.*, 1999]. Downwelling sky radiances were estimated spectrally for angles from 0° to 89° from zenith (step of 1°), and then they were integrated for the CE 312 channels. Equation (6) was fitted to the sky measurements to obtain the coefficient x_i and then effective angles were determined using equation (9). The effective atmospheric angles were also computed using the simulations for standard winter and summer midlatitude atmospheres for the four CE 312 channels. Angles of about 57° were obtained in both cases, which is slightly different to the value of about 53° given by Kondratyev [1969]. Figure 4 shows a comparison of the sky radiances measured and determined using equation (6) with the calculated x_i values for the CE 312 broad channel 1 and the narrow channel 3. Figure 4 shows the quite good correlation between simulated and measured atmospheric data, which proves the soundness of using equations (7) and (8) to estimate the sky irradiance.

[13] However, when reflection is specular, which is the usual approximation for the sea surface [Barton *et al.*, 1989], the reflection term can be rewritten as:

$$L_i^{ref}(\theta, \phi) = [1 - \varepsilon_i(\theta, \phi)]L_{i\ atm}^\downarrow(\theta, \phi \pm \pi) \quad (10)$$

[14] If the thermodynamic or kinetic skin temperature T is known, equations (1) to (10) allow the recovery of $\varepsilon_i(\theta, \phi)$ from radiometric measurements of $L_i(\theta, \phi)$ and $E_{i\ atm}^\downarrow \approx \pi \frac{2-x_i}{2-x_i} L_{i\ atm}^\downarrow(0^\circ) \approx \pi L_{i\ atm}^\downarrow(\theta_{ef})$ for a Lambertian reflecting surface as:

$$\varepsilon_i(\theta, \phi) = \frac{L_i(\theta, \phi) - E_{i\ atm}^\downarrow/\pi}{B_i(T) - E_{i\ atm}^\downarrow/\pi} \quad (11)$$

or $L_i(\theta, \phi)$ and $L_{i\ atm}^\downarrow(\theta, \phi \pm \pi)$ for a specular reflecting surface, as follows:

$$\varepsilon_i(\theta, \phi) = \frac{L_i(\theta, \phi) - L_{i\ atm}^\downarrow(\theta, \phi \pm \pi)}{B_i(T) - L_{i\ atm}^\downarrow(\theta, \phi \pm \pi)} \quad (12)$$

4. Measurement Strategy

[15] Measurements of the seawater surface and sky radiances ($L_i(\theta, \phi)$ and $L_{i\ atm}^\downarrow(\theta, \phi \pm \pi)$, respectively) were made with the radiometer CE 312 using a tripod with a graduated head. Zenith angles of 0° , 25° , 30° , 35° , 40° , 45° , 50° , 55° , 60° and 65° were used. Directions were measured with an inclinometer (accuracy of $\pm 0.01^\circ$). Each set of measurements took about 20 min and consisted of ten surface radiance measurements, one for each angle, using the four radiometer channels, alternately with ten sky observations for the same angles. An extra measurement was taken at 57° from zenith. Additionally, the six thermistors collected data every minute, which permitted us to obtain the concurrent temperature used to determine $B_i(T)$.

[16] A set of measurements was first carried out over a plane water surface (foam free) and then over a foam-covered water surface. The alternation of foam and foam-free measurements avoided important thermal stratification since the water was well stirred by the air flow of the diffusers. However, the skin temperature (T of equations (11) and (12)) can be slightly different to the temperature measured by the thermistors because of the skin effect, i.e., the difference between skin and subskin temperatures [Donlon *et al.*, 2002]. The temperature-depth profile depends on the wind speed and the net heat flux at the sea surface [Wick *et al.*, 1996; Fairall *et al.*, 1996] and may have differences larger than 1 K. However, the temperature difference seems to tend toward a constant value of about 0.2 K for wind speeds larger than 5–7 m/s [Konda *et al.*, 1994; Wick *et al.*, 1996; Murray *et al.*, 2000; Donlon *et al.*, 2002]. According to Donlon *et al.* [2002] this difference can be considered to be 0.17 ± 0.07 K for surface wind speed values ≥ 6 m/s and also during the night, i.e., when there are not vertical thermal gradients. Taking this fact into account, we considered this temperature difference and obtained the reference temperature T subtracting the constant temperature difference of 0.17 K from the temperatures measured by the thermistors.

[17] The foam coverage was nearly total during the foam measurements, with a 86% of small coated bubbles with a radius lower than 0.5 mm, and a 14% of bubbles of larger size with a mean radius of 0.8 mm (see Figure 3a). The foam layer thickness was 15 mm approximately (Figure 3b), and the bubble water coat thickness, which was measured from zooms of the vertical profiles, was in the 10–20 μm range [Camps *et al.*, 2005]. The thermal heads of the thermistors were inside the foam layer during the foam measurements, and we assumed their temperature as a reference.

[18] Taking into account the measurement strategy, the sky irradiance $E_{i\ atm}^\downarrow$ used in equation (11) was finally computed from the full set of sky measurements taken during each foam measurement. The sky measurements

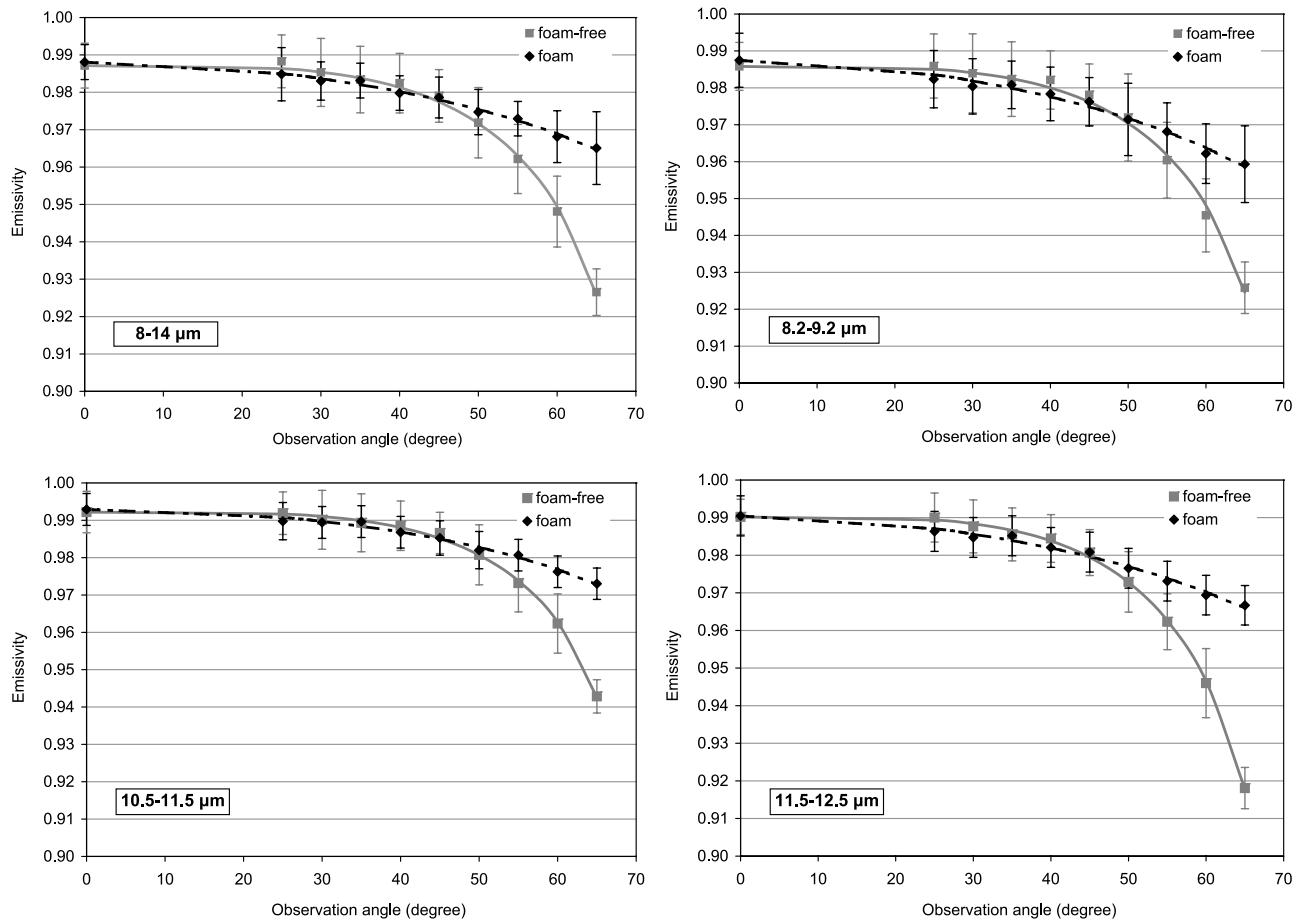


Figure 5. Measurements of the seawater emissivities as a function of the zenith observation angle for the four channels of the CE 312 radiometer for a foam-covered surface (dashed line) and a foam-free surface (solid line). The foam-covered surface has been considered a Lambertian reflector (equation (11)).

from 0° to 65° were fitted to equation (6) in order to obtain the coefficient x_i for each set of measurements, and then the sky irradiance was obtained using equation (7). The sky radiance measured at 57° was in good agreement with the sky irradiance divided by π (with a difference lower than 5% for all the cases). This fact was useful to assure the cloud-free condition for the atmosphere during the measurements used for the study, when equations (6)–(7) were suitable for the determination of the sky irradiance.

5. Results and Discussion

5.1. Foam Effect on the Sea Surface Emissivity

[19] TIR radiance measurements were used to obtain emissivity values for observation angles from 0° to 65° both for foam-covered and foam-free seawater surfaces. Figure 5 shows a comparison of the angular dependence of foam and foam-free emissivities. Foam-free emissivities were calculated using equation (12), since specular reflection can be considered for a plane water surface. However, Lambertian reflection was assumed for the case of a foam-covered surface, using equation (11) in this case. Figure 6 shows the results when specular reflection is considered also for the foam-covered surface, i.e., foam emissivities calculated with equation (12). Foam is considered a Lambertian reflector in the visible and near infrared spectrum

[Koepke, 1984], but no references have been found for the thermal infrared. We consider Lambertian reflection as more reasonable for the foam-covered surface in the thermal infrared region too, since multiple reflections produced by roughness could lead to an isotropic reflection behavior, without a predominant reflection direction.

[20] The plotted emissivities are average values for each angle. A total of twelve set of measurements (as defined in section 4) were taken for each case, which were measured under totally cloud-free atmospheres to avoid cloud cover influences. Data with high variability in the temperatures measured by the thermistors were refused. The error bars shown in the figures are the maximum values between standard deviations and average measurement errors. Measurement errors were obtained applying error propagation to equations (11) and (12) and taking into account three error sources: (1) the CE 312 radiometric uncertainty for each channel, (2) the calibration equation error for each channel, and (3) the uncertainty in the temperature measured by the thermistors (± 0.1 K). Average emissivity errors of ± 0.004 , ± 0.005 , ± 0.004 , ± 0.006 were estimated for channels 1–4, respectively. However, taking into account the difficulty of estimating the skin temperature from the subskin temperature measured by the thermistors, especially for the foam case, maybe larger T uncertainties could be used in the

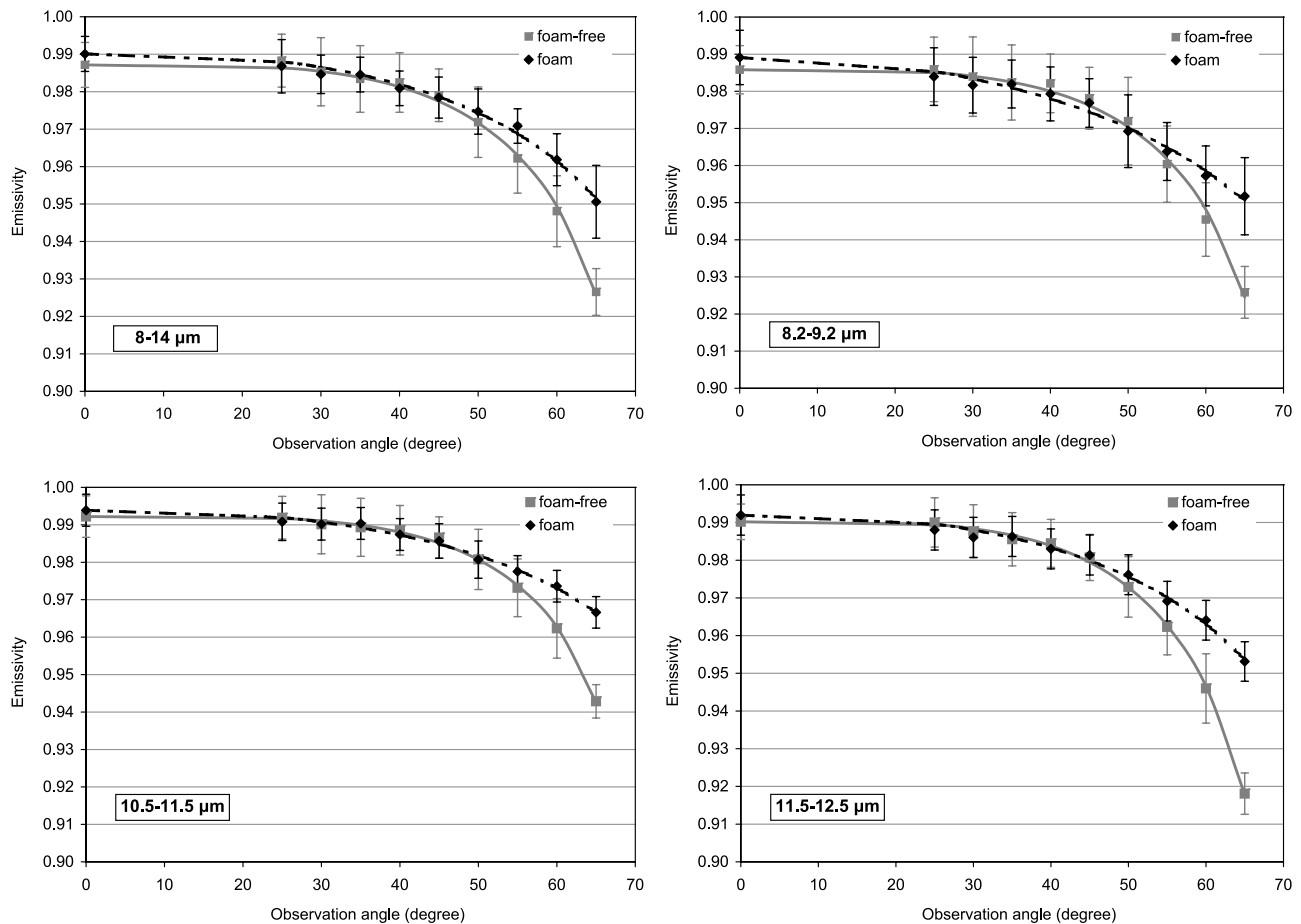


Figure 6. The same as Figure 5 but assuming specular reflection for the foam-covered surface (equation (12)).

propagation of errors, for example, ± 0.3 K. Emissivity errors of ± 0.007 , ± 0.007 , ± 0.006 , ± 0.009 for channels 1–4, respectively, were obtained when a T uncertainty of ± 0.3 K was considered, which were still equal or lower than the standard deviations shown in Figures 5 and 6.

[21] Both Figures 5 and 6 show a significant effect of foam on emissivity at large observation angles, even though different reflection assumptions are considered. The four CE 312 channels show a decrease of the emissivity angular dependence. There is still an emissivity decrease with angle, but foam emissivity values are much larger than foam-free emissivities at observation angles larger than 50° . However, differences between foam and foam-free emissivities are within the experimental errors at small observation angles, i.e., up to about 45° . This behavior is shown both when the Lambertian or the specular reflection is considered to calculate the emissivity through equations (11) and (12). The foam effect appears to be larger when Lambertian reflection is considered (Figure 5). For example, differences between foam and foam-free emissivities assuming a Lambertian reflecting foam are 0.039 ± 0.007 , 0.049 ± 0.008 , 0.030 ± 0.007 , and 0.033 ± 0.008 at 65° for channels 1 to 4, respectively, but considering a specular reflecting foam these differences are 0.024 ± 0.008 , 0.035 ± 0.009 , 0.024 ± 0.007 , and 0.026 ± 0.010 for channels 1 to 4, respectively.

However, the foam effect is evident at large observation angles in any case.

[22] On the other hand, Figure 5 shows a small negative difference between foam and foam-free emissivities at low observation angles, but the difference is opposite for observation angles larger than 45° – 55° , where foam emissivities are significantly larger than foam-free values. Although the differences for small angles are lower than the emissivity error bars, we can notice that this behavior was observed previously when the effect of surface wind on seawater emissivity was analyzed [Wu and Smith, 1997; Niclòs et al., 2005]. Figure 7 shows the sea surface emissivities determined by the model of Wu and Smith [1997] for wind speed values of 0 m/s and 15 m/s. Surface wind produces roughness on the sea surface, which was characterized by Cox and Munk [1954] using an approximately normal and isotropic facet slope distribution. Wu and Smith [1997] considered this facet slope distribution to model the sea surface emissivity under several wind speed conditions, taking into account also the effect of multiple surface reflections. Figure 7 shows how the wind-induced roughness decreases slightly the emissivity up to an observation angle of about 58° and then increases it for larger observation angles. The similarity between wind and foam effects suggests that foam coverage produces roughness, and thus it generates an important alteration of the slope distribution,

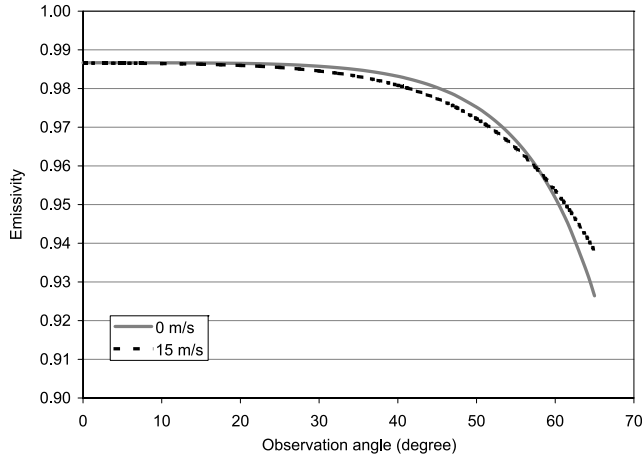


Figure 7. Angular dependence of the sea surface emissivity calculated using the model of *Wu and Smith* [1997] for the CE 312 channel 1 (8–14 μm) and for wind speed values of 0 m/s (solid line) and 15 m/s (dashed line).

which is probably the major cause of the seawater emissivity change.

[23] Taking into account the dependence of the difference between foam and no-foam emissivities on observation angle, a mathematical function can be proposed in terms of $\sec(\theta) - 1$. Figure 8 shows the emissivity differences against $\sec(\theta) - 1$ for the four CE 312 channels (Lambertian reflection assumed). Values around 0.02 and 0.04 are obtained at 60° and 65° , respectively. A quadratic function was determined for each channel:

$$\varepsilon_{i,\text{foam}}(\theta) - \varepsilon_{i,\text{foam-free}}(\theta) = a_i[\sec(\theta) - 1]^2 + b_i[\sec(\theta) - 1] + c_i \quad (13)$$

Table 1 shows the coefficients a_i , b_i , and c_i for each channel, together with the error of estimate, σ_i , and the coefficient of determination, r_i^2 . This equation permits to estimate the magnitude of the foam effect with angle as a function of the TIR spectral band, showing that the effect is the largest in 11.5–12.5 μm and the lowest in 10.5–11.5 μm .

5.2. Implications in the Sea Surface Temperature Retrieval From Satellite

[24] The most common algorithm for SST retrieval from satellite is the split window technique, which takes advantage of the different absorption between two bands placed within the atmospheric window 10–12.5 μm for performing the atmospheric correction [McMillin, 1975]. This section shows the foam effect on the SST retrieval from satellite when this technique is used, taking into account how foam modifies the sea surface emissivity.

[25] The emissivity correction in the split window technique can be written in terms of temperature as [Coll and Caselles, 1994, 1997]:

$$\Delta T_{EC_SW}(\theta, W) = \alpha(W)(1 - \varepsilon(\theta)) - \beta(W)\Delta\varepsilon(\theta) \quad (14)$$

where $\varepsilon(\theta)$ and $\Delta\varepsilon$ are the average and the difference of emissivities for the split window bands. Taking into

account the close similarity between CE 312 channels 3 and 2 and the spectral bands 4 and 5 of the NOAA-AVHRR/3, equation (14) was evaluated for this satellite radiometer where $\varepsilon(\theta) = (\varepsilon_4(\theta) + \varepsilon_5(\theta))/2$ and $\Delta\varepsilon = \varepsilon_4(\theta) - \varepsilon_5(\theta)$ were considered. $\alpha(W)$ and $\beta(W)$ are coefficients dependent on the atmospheric properties [Coll and Caselles, 1997; Niclòs et al., 2007]. A cloud-free, latitude equally distributed database of 402 radiosoundings (SAFREE) [François et al., 2002] was used to determine the atmospheric magnitudes involved in these coefficients. These magnitudes were simulated with the radiative transfer code MODTRAN 4 [Berk et al., 1999] for angles up to 65° and then $\alpha(W)$ and $\beta(W)$ were calculated for the AVHRR/3.

[26] Figure 9 shows the difference between the emissivity correction of the split window technique (equation (14)) using foam-free and foam emissivities, as a function of water vapor content and observation angle. Foam-free emissivities were determined by the model of *Wu and Smith* [1997] and integrated for the AVHRR/3 channels 4 and 5. Foam emissivities were calculated from the foam-free values using equation (13) and the coefficients given in Table 1 for the CE 312 channels 3 and 2. Figure 9 shows that SST differences up to 1.2 K are obtained using the split window technique because of the emissivity modification by foam.

[27] Additionally, the foam effect on SST when a single-channel equation is used was estimated for comparison, showing that the foam coverage can cause SST differences larger than 1.5 K and 2.5 K for bands at 10 and 11 μm , respectively, at large observation angles (for which the emissivity increase with foam can be 0.04).

[28] Therefore the foam effect on the SST determination from satellite is negligible for observation angles up to 45° – 50° , but it yields important SST differences at large observation angles. These differences are much larger than the accuracy currently required for applications in both climate monitoring and operational oceanography (± 0.3 K) [Barton, 1992], and thus they should be taken into account.

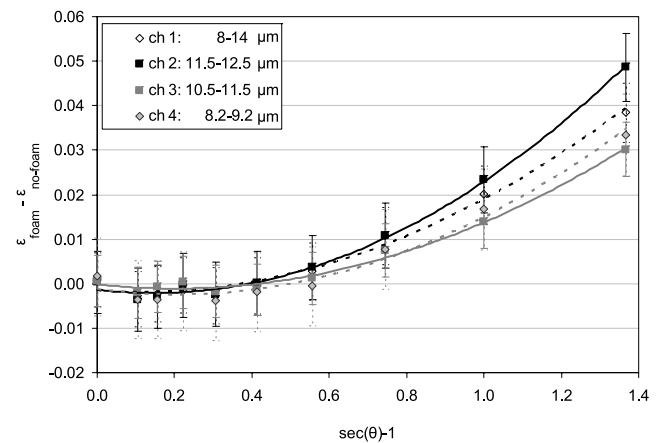


Figure 8. Difference between foam and foam-free emissivities, $\varepsilon_{i,\text{foam}}(\theta) - \varepsilon_{i,\text{foam-free}}(\theta)$, against $\sec(\theta) - 1$, where θ is the observation angle. The quadratic regression functions obtained for each channel are also plotted (lines). The foam emissivities were calculated using equation (11).

Table 1. Coefficients a_i , b_i , and c_i of Equation (13) for the CE 312 Channels^a

CE 312 Channel	Wavelength, μm	a_i	b_i	c_i	σ_i	r_i^2
1	8–14	0.026	−0.006	−0.0015	0.0018	0.987
4	8.2–9.2	0.034	−0.010	−0.0014	0.0012	0.996
3	10.5–11.5	0.023	−0.009	−0.0002	0.0012	0.989
2	11.5–12.5	0.028	−0.011	−0.0012	0.002	0.979

^aErrors of estimate, σ_i , and coefficients of determination, r_i^2 , are also included.

5.3. Application to Open Sea Conditions

[29] In order to check the goodness of the artificially generated foam as compared to natural foam encountered over the sea after a wave splash, 80 photographs of sea surface (with a salinity of 33.8 psu) were acquired in the coasts of the Gran Canaria island after wave breaking [Camps *et al.*, 2005]. Figure 3c shows the structure and foam layer thickness, which is even larger than it during the controlled experiment (see also Figure 3b). Additionally, the average radius of the artificially generated bubbles during our experiment (salinity of 34 psu) was of about 0.5 mm, similar to the radius of the bubbles naturally generated in the sea [Camps *et al.*, 2005]. Therefore the results obtained for our experiment can be applied to natural sea conditions.

[30] Random foam patches are generated in open sea conditions and the foam coverage is hardly ever total. As we have determined the angular variation of the emissivity for nearly total foam coverage ($\varepsilon_{i,foam}(\theta)$), the thermal infrared effective emissivity for a foam partially covered surface can be estimated as follows:

$$\varepsilon_i(\theta) = F_{foam}\varepsilon_{i,foam}(\theta) + (1 - F_{foam})\varepsilon_{i,foam-free}(\theta) \quad (15)$$

where F_{foam} is the fraction of the sea covered by foam. Taking into account the proposed equation for the calculation of the difference between foam and foam-free emissivities (equation (13)), equation (15) can be rewritten as:

$$\varepsilon_i(\theta) = \varepsilon_{i,foam-free}(\theta) + F_{foam} [a_i[\sec(\theta) - 1]^2 + b_i[\sec(\theta) - 1] + c_i] \quad (16)$$

which requires the coefficients included in Table 1 and foam-free emissivity values.

[31] For example, for a fraction of foam coverage of $F_{foam} = 0.25$ (25%), the effective emissivity is 1% larger than the value for a foam-free surface at an observation angle of 65° , which could yield SST uncertainties larger than ± 0.3 K even when a split window technique is used. This difference is of about 2%, 3–4%, and 4–5% for foam coverage percentages of 50%, 75% and 100%, which could yield uncertainties larger than ± 0.6 K, ± 0.9 K and ± 1.2 K, respectively.

[32] Consequently, the correction of foam effect on the emissivity in the thermal infrared region can be possible if the fraction of sea covered by foam is known. Therefore its effect on the SST could be also corrected, improving the accuracy of the SST retrieval from satellite.

[33] Foam coverage and layer thickness are wind-dependent in open sea conditions. The fraction of the sea

covered by foam can be related with the surface wind speed. There are a large number of publications regarding this issue, which proposed experimental fitting functions such as:

$$F_{foam} = \chi U_{10m}^\delta \quad (17)$$

where χ and δ are coefficients determined experimentally (δ is typically around 3) and U_{10m} is the surface wind speed at 10 m [Monahan, 1971; Monahan and O’Muircheartaigh, 1980; Spillane *et al.*, 1986; Marks, 1987; Hanson and Phillips, 1999; Camps *et al.*, 2002, 2004; Lafon *et al.*, 2004]. Traditionally, the foam fraction is determined from photographs or video images of the sea state collected from ocean research platforms. For example, Camps *et al.* [2002] obtained this sort of expression by means of the analysis of 20,000 photographs of the sea surface taken from an oilrig during the Wind and Salinity Experiment 2000 (WISE 2000) carried out as a SMOS Mission experimental campaign. Monahan and Woolf [1989] discriminated the coverage of different whitecaps states (crest foam and static foam) and also suggested dependence on the atmospheric stability through the air-sea temperature difference, ΔT , as:

$$F_{foam} = \chi U_{10m}^\delta \exp(\gamma \Delta T) \quad (18)$$

γ being another fitting coefficient.

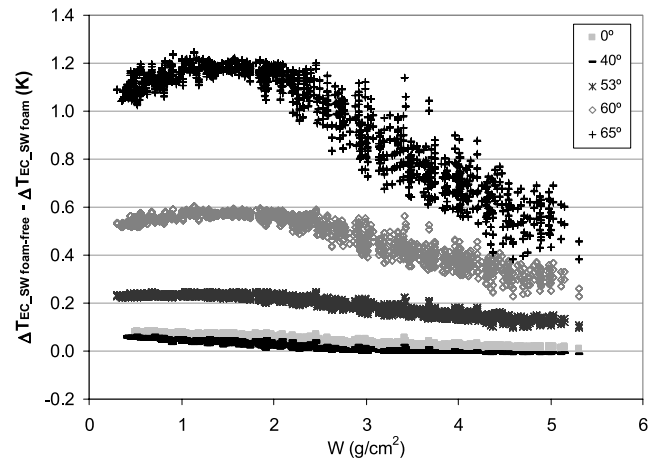


Figure 9. Difference in the emissivity correction for a split window technique applied to the AVHRR/3 when foam-free and foam emissivities are considered (equation (14)) as a function of the column water vapor content and the observation angle.

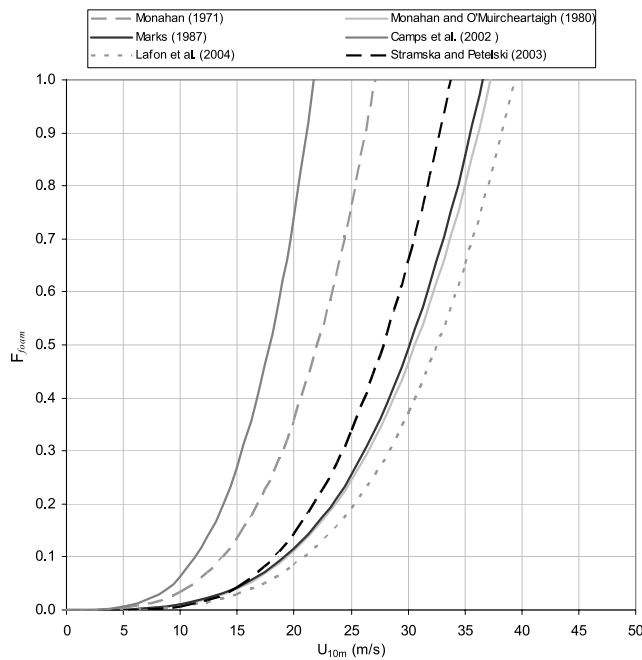


Figure 10. Comparison of some of the empirical equations given in the bibliography in order to determine the foam coverage as a function of the surface wind speed at 10 m, U_{10m} .

[34] Other authors [Bondur and Sharkov, 1982; Monahan, 1993; Asher et al., 2002; Stramska and Petelski, 2003] proposed a slightly different equation, where the foam coverage was a function of:

$$F_{foam} = f \left[\chi' (U_{10m} - \gamma')^{\delta'} \right] \quad (19)$$

where γ' is now the threshold wind speed for whitecaps formation. Figure 10 shows a comparison of some of the equations proposed for the foam fraction estimate as a function of the wind speed.

[35] Imagery of wind speed is currently provided by microwave sensors such as: the Advanced Synthetic Aperture Radar (ASAR) on board ENVISAT, the Advanced Microwave Scanning Radiometer for EOS (AMSR-E) on EOS Aqua, the Advanced Scatterometer (ASCAT) on board MetOp-A, the altimeter Poseidon 2 on Jason 1, and the scatterometer QuikScat of NASA (free data available on <http://www.ssmi.com>). These data could be used in the proposed equations to obtain the foam coverage from satellite.

[36] Recently, Anguelova and Webster [2006] have reviewed the existing equations for the foam fraction estimate, showing the existence of some discrepancies and the possible dependence on other magnitudes. They suggest a new method to retrieve the foam coverage from routine satellite measurements in the microwave spectrum as an alternative to the traditional photographic measurements.

[37] Therefore there are several methods to obtain the foam fraction required in order to determine the foam effect in terms of sea surface emissivity by means of equation (16). However, the estimated foam coverage depends on the used

method at the moment. More work is required in the modeling and the determination of the foam coverage from satellite in order to improve the SST estimate by correcting the foam effect on the surface emissivity.

6. Conclusions

[38] This study shows the effect of foam on seawater emissivity for observation angles from 0° to 65° . At low observation angles, the effect of foam is negligible, always lower than the measurement errors. This conclusion is in accordance with the measurements at 10° carried out by Salisbury et al. [1993]. However, the foam influence is significant at large observation angles ($>45^\circ$), with larger emissivities for foam-covered surfaces. The foam effect is to reduce the angular variation of seawater emissivity. The difference between foam and foam-free emissivities increases with angle. Emissivity differences from 0.03 to 0.05 are obtained at 65° , depending on the spectral band. These values are 1 order of magnitude larger than the emissivity measurement errors and cannot be neglected in the retrieval of seawater temperatures from radiometric measurements taken over foam-covered surfaces, since errors larger than 1.2 K can be obtained even using a split window technique, which is four times larger than the minimum accuracy of ± 0.3 K currently required for the SST in climate and oceanography applications.

[39] A relationship has been proposed to estimate the emissivity for foam-covered seawaters from the foam-free emissivity values, which can be directly measured or provided by models. This expression gives the emissivity for a completely foam-covered surface. However, this is not the usual case in open sea conditions. We propose the use of an effective emissivity for partially foam-covered surfaces, which requires an estimate of the fraction of the sea covered by foam. Although there are a large number of papers dealing with this issue, the discrepancies in the results suggest that more work is necessary for an accurate estimate of the foam coverage from satellite.

[40] According to our results, the correction of the effect of the foam coverage could improve the accuracy of SST determination from satellite.

[41] **Acknowledgments.** This work has been supported by the Spanish Ministerio de Educación y Ciencia (projects REN2003-09771/CLI, CGL2004-06099-C03-01/CLI, and CGL2005-24207-E/CLI and Juan de la Cierva research contract of R. Niclòs). The authors wish to thank the assistance of Adriano Camps, Ramón Villarino, and Jorge Miranda during the FROG-2003 campaign. Thanks are also given to the IRTA personnel for their help during the experiment at their facilities.

References

- Anguelova, M. D., and F. Webster (2006), Whitecap coverage from satellite measurements: A first step toward modeling the variability of oceanic whitecaps, *J. Geophys. Res.*, *111*, C03017, doi:10.1029/2005JC003158.
- Asher, W., J. Edson, W. McGillis, R. Wanninkhof, D. Ho, and T. Litchendorf (2002), Fractional area whitecap coverage and air-sea gas transfer velocities measured during GasEx-98, in *Gas Transfer at Water Surfaces*, *Geophys. Monogr. Ser.*, vol. 127, edited by M. Donelan et al., pp. 199–204, AGU, Washington, D. C.
- Barton, I. J. (1992), Satellite-derived sea surface temperatures: A comparison between operational, theoretical and experimental algorithms, *J. Appl. Meteorol.*, *31*, 432–442.
- Barton, I. J., A. M. Zavody, D. M. O'Brien, D. R. Cutten, R. W. Saunders, and D. T. Llewelling-Jones (1989), Theoretical algorithms for satellite-derived sea surface temperatures, *J. Geophys. Res.*, *94*, 3365–3375.

- Berk, A., G. P. Anderson, P. K. Acharya, J. H. Chetwynd, L. S. Bernstein, E. P. Shettle, M. W. Matthew, and S. M. Adler-Golden (1999), *MODTRAN 4 User's Manual*, 95 pp., Air Force Res. Lab., Space Vehicles Dir., Air Force Mater. Command, Hascom Air Force Base, Mass.
- Bondur, V., and E. Sharkov (1982), Statistical properties of whitecaps on a rough sea, *Oceanography*, *22*, 274–279.
- Camps, A., et al. (2002), Sea surface emissivity observations at L-band: First results of the Wind and Salinity Experiment WISE-2000, *IEEE Trans. Geosci. Remote Sens.*, *40*, 2117–2130.
- Camps, A., et al. (2004), The WISE 2000 and 2001 field experiments in support of the SMOS mission: Sea surface L-band brightness temperature observations and their application to sea surface salinity retrieval, *IEEE Trans. Geosci. Remote Sens.*, *42*, 804–823.
- Camps, A., et al. (2005), The emissivity of foam-covered water surface at L-band: Theoretical modeling and experimental results from the FROG 2003 field experiment, *IEEE Trans. Geosci. Remote Sens.*, *43*, 925–937.
- Coll, C., and V. Caselles (1994), Analysis of the atmospheric and emissivity influence on the split-window equation for sea surface temperature, *Int. J. Remote Sens.*, *15*, 1915–1932.
- Coll, C., and V. Caselles (1997), A split-window algorithm for land surface temperature from advanced very high resolution radiometer data: Validation and algorithm comparison, *J. Geophys. Res.*, *102*, 16,697–16,713.
- Cox, C., and W. Munk (1954), Some problems in optical oceanography, *J. Mar. Res.*, *14*, 63–78.
- Dombrovskiy, L. A., and V. Y. Raizer (1992), Microwave model of a two-phase medium at the ocean surface, *Atmos. Oceanic Phys.*, *28*, 650–656.
- Donlon, C. J., P. J. Minnet, C. Gentemann, T. J. Nightingale, I. J. Barton, B. Ward, and M. J. Murray (2002), Toward improved validation of satellite sea surface skin temperature measurements for climate research, *J. Clim.*, *15*, 353–369.
- Fairall, C. W., E. F. Bradley, J. S. Godfrey, G. A. Wick, J. B. Edson, and G. S. Young (1996), Cool-skin and warm-layer effects on sea surface temperature, *J. Geophys. Res.*, *101*, 1295–1308.
- François, C., A. Brisson, P. LeBorgne, and A. Marsouin (2002), Definition of a radio-sounding database for sea surface brightness temperature simulations: Applications to sea surface temperature retrieval algorithm determination, *Remote Sens. Environ.*, *81*, 309–326.
- Hanson, J., and O. Phillips (1999), Wind sea growth and dissipation in the open ocean, *J. Phys. Oceanogr.*, *29*, 1633–1648.
- Koepke, P. (1984), Effective reflectance of oceanic whitecaps, *Appl. Opt.*, *23*, 1816–1824.
- Konda, M., N. Imasato, K. Nishi, and T. Toda (1994), Measurement of the sea surface emissivity, *J. Oceanogr.*, *50*, 17–30.
- Kondratyev, K. T. (1969), *Radiation in the Atmosphere*, Academic, New York.
- Lafon, C., J. Piazzola, P. Forget, O. le Calve, and S. Despiau (2004), Analysis of the variations of the whitecap fraction as measured in a coastal zone, *Boundary Layer Meteorol.*, *111*, 339–360.
- Legrand, M., C. Pietras, G. Brogniez, M. Haeffelin, N. K. Abuhassan, and M. Sicard (2000), A high-accuracy multiwavelength radiometer for in situ measurements in the thermal infrared. Part 1: Characterization of the instrument, *J. Atmos. Oceanic Technol.*, *17*, 1203–1214.
- Marks, F. (1987), Marine aerosols and whitecaps in the North Atlantic and Greenland Sea regions, *Dtsch. Hydrogr. Z.*, *40*, 71–79.
- McMillin, L. M. (1975), Estimation of sea surface temperatures from two infrared window measurements with different absorption, *J. Geophys. Res.*, *80*, 5113–5117.
- Monahan, E. (1971), Oceanic whitecaps, *J. Phys. Oceanogr.*, *1*, 139–144.
- Monahan, E. (1993), Occurrence and evolution of acoustically relevant subsurface bubble plumes and their associated, remotely monitorable, surface whitecaps, in *Natural Physical Sources of Underwater Sound*, edited by B. Kerman, pp. 503–517, Springer, New York.
- Monahan, E., and I. G. O'Muircheartaigh (1980), Optimal power-law description of oceanic whitecaps coverage dependence on wind speed, *J. Phys. Oceanogr.*, *10*, 2094–2099.
- Monahan, E., and D. Woolf (1989), Comments on “Variations of whitecap coverage with wind stress and water temperature,” *J. Phys. Oceanogr.*, *19*, 706–709.
- Murray, M. J., M. R. Allen, C. J. Merchant, A. R. Harris, and C. J. Donlon (2000), Direct observations of skin-bulk SST variability, *Geophys. Res. Lett.*, *27*, 1171–1174.
- Niclòs, R., V. Caselles, C. Coll, and E. Valor (2004), Autonomous measurements of sea surface temperature using in situ thermal infrared data, *J. Atmos. Oceanic Technol.*, *21*, 683–692.
- Niclòs, R., E. Valor, V. Caselles, C. Coll, and J. M. Sánchez (2005), In situ angular measurements of thermal infrared sea surface emissivity: Validation of models, *Remote Sens. Environ.*, *94*, 83–93.
- Niclòs, R., V. Caselles, C. Coll, and E. Valor (2007), Determination of sea surface temperature at large observation angles using an angular and emissivity-dependent split-window equation, *Remote Sens. Environ.*, *111*, 107–121.
- Rubio, E., V. Caselles, and C. Badenas (1997), Emissivity measurements of several soils and vegetation types in the 8–14 μm wave band: Analysis of two field methods, *Remote Sens. Environ.*, *59*, 490–521.
- Salisbury, J. W., D. M. D'Aria, and F. F. Sabins (1993), Thermal infrared remote sensing of crude oil slicks, *Remote Sens. Environ.*, *45*, 225–231.
- Spillane, M., E. Monahan, P. Bowyer, D. Doyle, and P. Stabeno (1986), Whitecaps and global fluxes, in *Oceanic Whitecaps and Their Role in Air-Sea Exchange Processes*, edited by E. Monahan and G. Niocaill, pp. 209–218, Springer, New York.
- Stramska, M., and T. Petelski (2003), Observations of oceanic whitecaps in the north polar waters of the Atlantic, *J. Geophys. Res.*, *108*(C3), 3086, doi:10.1029/2002JC001321.
- Ulaby, F. T., R. K. Moore, and A. K. Fung (1986), *Microwave Remote Sensing, Active and Passive*, vol. III, *From Theory to Applications*, 2162 pp., Artech House, Norwood, Mass.
- Watts, P. D., M. R. Allen, and T. J. Nightingale (1996), Wind speed effects on sea surface emission and reflection for the Along Track Scanning Radiometer, *J. Atmos. Oceanic Technol.*, *13*, 126–141.
- Wick, G. A., W. J. Emery, L. H. Kantha, and P. Schlüssel (1996), The behavior of the bulk-skin sea surface temperature difference under varying wind speed and heat flux, *J. Phys. Oceanogr.*, *26*, 1969–1988.
- Wu, X., and W. L. Smith (1997), Emissivity of rough sea surface for 8–13 μm : Modelling and verification, *Appl. Opt.*, *36*, 2609–2619.

V. Caselles, C. Coll, and E. Valor, Department of Earth Physics and Thermodynamics, University of Valencia, 50 Dr. Moliner, E-46100 Burjassot, Spain.

R. Niclòs, Meteorology Department, Mediterranean Centre for Environmental Studies, 14 Charles Darwin, E-46980 Paterna, Spain. (raquel.niclos@uv.es)